Astron. Astrophys. 344, 221–230 (1999)

ASTRONOMY AND ASTROPHYSICS

Photospheric metal abundances of AR Lacertae⋆

Thomas Gehren[1], **Renate Ottmann**[2], **and Johannes Reetz**[1]

[1] Institut für Astronomie und Astrophysik der Universität München, Scheinerstrasse 1, D-81679 München, Germany
[2] Max-Planck-Institut für Extraterrestrische Physik, Giessenbachstrasse, D-85740 Garching, Germany

Received 6 November 1998 / Accepted 7 January 1999

Abstract. High-resolution spectra of the RS CVn system AR Lac taken during total eclipse of the primary component lead to a precise determination of the stellar effective temperature of the secondary, $T_{eff} = 5100 \pm 100$ K, and a surface gravity $\log g = 3.65 \pm 0.1$. The small-scale motions are well represented by a microturbulence velocity of $v_t = 1.6 \pm 0.3\,\mathrm{km\,s^{-1}}$. Examination of a number of spectral windows by means of spectrum synthesis based on solar spectrum reference fits produces a pattern of photospheric metal abundances that is essentially represented by solar or slightly enhanced values. This is at variance with the subsolar metal abundances reported from X-ray observations with the ROSAT and ASCA satellites.

The effective temperature determined here restricts the surface fraction of cool matter such as confined in star spots during the present observations to values around 0.3. For a close binary system with an active chromosphere the photospheric spectra are normal. No spectrum variations on a half hour time scale are detected.

Key words: stars: starspots – stars: individual: AR Lac – stars: coronae – stars: binaries: eclipsing – stars: abundances

1. Introduction

AR Lac is one of the brightest and therefore most well-observed eclipsing active binary systems consisting of a close pair of stars in very similar stages of evolution. The primary component is the less evolved G2 IV subgiant[1]; it is totally eclipsed every 2 days by the secondary, a K0 IV subgiant. The system is close enough to have a circular orbit, and it should also be very near to co-rotation. It is particularly well-known for its chromospheric and coronal activity documented by the results of the HEAO2, EXOSAT, ROSAT, EUVE and ASCA missions (e.g. Walter et al. 1983, White et al. 1990, Ottmann et al. 1993, Patterer et al. 1993, Kaastra et al. 1996). The surfaces of both stars are covered with spots that are assumed to document the existence of magnetic fields, chromospheric and coronal activity in much the same way as in the Sun (Kron 1947, Eaton & Hall 1979, Poe & Eaton 1985, Solanki 1996, Lanza et al. 1998).

The more recent analyses of X-ray spectra observed with the ROSAT, ASCA and EUVE satellites have considerably extended our knowledge of these systems. One of the more exciting results was that the coronae of RS CVn stars apparently harbour subsolar element abundances, sometimes comparable with abundances found in the oldest Galactic disk stars. Thus, AR Lac was reported to show spectral features of the more important metals requiring abundances 4 times lower than solar photospheric (or meteoritic) values (White et al. 1994, Singh et al. 1996, Kaastra et al. 1996). This has led Ottmann et al. (1998) to look for evidence of a metallicity gradient in the outer atmospheres of a number of RS CVn stars using phase-resolved high-resolution spectroscopy. For II Peg and λ And, the two binaries among their sample with published coronal abundances, the *differences* with respect to the photospheric metal abundances amount to $\Delta\,[\mathrm{Fe/H}] \approx -0.8$, significantly above any observational errors of high resolution spectroscopy or the uncertainties of spectrum analysis, whereas the photospheric abundances themselves were found at most a factor of 2 different from solar. In direct comparison with the *solar* corona it is evident that such an underabundance contradicts any simple interpretation such as the *first ionization potential* effect (FIP, Meyer 1985).

While spectral modeling of these stars required only a *single* atmospheric contribution together with an *a priori* unknown contribution from starspots, self-consistent synthesis of AR Lac spectra doubles the input from two stellar surfaces with correspondingly different spot contributions. The notable exception to this constellation is, however, the short stellar eclipse of AR Lac's primary. Our present approach to photospheric element abundances is thus applied to a series of 3 short-exposure spectra taken during total eclipse of the primary component of AR Lac. Although most likely a snapshot of the ever-varying photospheric surface we believe that the photospheric abundances obtained from these spectra are independent of the particular binary configuration, a notion that is confirmed during the analysis.

In the following section we comment on the observations obtained with the FOCES échelle spectrograph. The secondary's

Send offprint requests to: T. Gehren (gehren@usm.uni-muenchen.de)

⋆ Based on observations collected at the German-Spanish Astronomical Center, Calar Alto, Spain

[1] Following past conventions, we refer to the G2 IV component as the *primary* although it is the optically fainter, less luminous, less massive and less evolved star

Table 1. The RS CVn-type binary system AR Lac. Index "1" refers to the primary

RA (2000)	$22^{\rm h}\,08^{\rm m}\,41.07^{\rm s}$	
DEC (2000)	$+45^\circ\,44'\,29.1''$	
SpT	K0 IV + G2 IV	Walter et al. 1983
$m_{\rm V}$	6.11	outside eclipse
π	23.79 ± 0.59 mas	HIPPARCOS 1997
V_0	$-33 \pm 2\,{\rm km\,s^{-1}}$	Popper 1990
T_0	JD 2 426 623.844	epoch of zero longitude
P	1.983222 days	Hall & Kreiner 1980
i	$87^\circ \pm 1^\circ$	Chambliss 1976
a	4.538 $R_\odot$	Sanford 1951
$\rm M_{V,1}$	4.0	Popper 1990
$\rm M_{V,2}$	3.6	
K_1	$117 \pm 2\,{\rm km\,s^{-1}}$	
K_2	$113 \pm 2\,{\rm km\,s^{-1}}$	
M_1	$1.23 \pm 0.05\ M_\odot$	
M_2	$1.27 \pm 0.05\ M_\odot$	
$R_{\star,1}$	$1.52 \pm 0.04\ R_\odot$	
$R_{\star,2}$	$2.72 \pm 0.10\ R_\odot$	

fundamental parameters are determined in Sect. 3 taking account of a possible contamination by star spots; this section also describes spectrum synthesis based on model atmosphere techniques. Finally, we discuss the synthesis results and their reliability in the last section with a short excursion to spectrum variations.

2. Observations and data reduction

The basic data of the eclipsing binary system AR Lac are from Sanford (1951), but Table 1 gives some more recent updates from Popper (1990) and other references. It should also be noted that AR Lac is a system with significant period variations (Hall et al. 1976, Gunn et al. 1996, Jetsu et al. 1997).

The observations discussed here have been obtained under extremely unfavourable weather conditions with the fibre optics Cassegrain échelle spectrograph FOCES at the 2.2m telescope of the DSAZ on Calar Alto. Three exposures of 15 min each have been taken during total eclipse of the secondary. They were all recorded with a 1024^2 Tektronix CCD with a 2-pixel ($48\,\mu$m) resolution of $R = 40\,000$. The signal-to-noise ratio is approximately 200 in the red but reaches only 100 near the G band. The spectra are flatfield-calibrated with a halogen lamp spectrum, and put on a proper wavelength scale with a dispersion solution obtained from a Th-Ar lamp exposure. The scrambling of the light rays in the fibre coupling the Cassegrain focal plane with the spectrograph results in two important advantages as compared with other instruments,

– The flatfield calibration produces really a *flat* spectral continuum with virtually *no* modulation left except the ratio of flux temperatures from object (AR Lac) and halogen lamp. For each single order this ratio varies by less then 2% of the continuum flux.

Table 2. Echelle spectra of AR Lac obtained during total eclipse of the secondary at August 28, 1996 (JD 2 450 323.5 + ET)

Exposure	63	64	65
UT	$03^{\rm h}\,08^{\rm m}\,08^{\rm s}$	$03^{\rm h}\,27^{\rm m}\,25^{\rm s}$	$03^{\rm h}\,45^{\rm m}\,43^{\rm s}$
V_{rad}	$-37.2\,{\rm km\,s^{-1}}$	$-41.3\,{\rm km\,s^{-1}}$	$-46.4\,{\rm km\,s^{-1}}$
$\sigma(V_{rad})$	$1.2\,{\rm km\,s^{-1}}$	$1.1\,{\rm km\,s^{-1}}$	$1.4\,{\rm km\,s^{-1}}$

– The spectrograph is detached from the telescope thus allowing an extremely precise wavelength calibration. Recent results (Pfeiffer et al. 1998) have demonstrated that the wavelength scale of a single échelle order is reproducible within an *rms* error of only 2 to 4 mÅ. Thus unresolved stellar absorption lines allow a radial velocity determination of $\sim 0.25\,{\rm km\,s^{-1}}$ in a single spectral order; using the whole set of between 60 and 80 échelle orders the error of the mean can be as small as $0.02\,{\rm km\,s^{-1}}$. However, such numbers cannot be obtained with spectra of AR Lac, since the absorption lines are broadened by a rotational velocity of more than $70\,{\rm km\,s^{-1}}$.

The order spectra were reduced and combined using the available order overlap information. Tests of control objects (mostly extremely metal-poor halo stars) demonstrate the flatness of the continuum after flatfield calibration. The exposure data are assembled in Table 2. The rotational velocity as measured from spectrum synthesis of medium and strong lines (cf. next section) is $v_{rot} = 73 \pm 3\,{\rm km\,s^{-1}}$. This is substantially lower than the unpublished $81\,{\rm km\,s^{-1}}$ of Fekel (1998, see the catalogue of Strassmeier et al. 1993); it fits perfectly to the $72\,{\rm km\,s^{-1}}$ cited in Huenemoerder & Ramsey (1984) but is somewhat higher than would be obtained in the case of co-rotation, where the data in Table 1 suggest a value around $69\,{\rm km\,s^{-1}}$. The accuracy of our fits is significant; thus a value as high as $81\,{\rm km\,s^{-1}}$ must be ruled out for simple flux-convolved profile fits, and if co-rotation were assumed to be valid the radius of the secondary should be around $R = 2.85\ R_\odot$ instead of $2.72\ R_\odot$ as given by Popper (1990). Such a radius would still fit to the surface gravity determined by spectrum synthesis, $\log g = 3.65$ (compared with $\log g = 3.67$ found in Table XXXVIII of Popper).

As noted in Table 2 the radial velocity varied by roughly $10\,{\rm km\,s^{-1}}$ over a time interval of 37 min, in full accordance with the predicted orbit. The most precise determinations are obtained in the red using the *terrestrial* lines of H_2O from which we find $\dot V_{rad} = 0.0040 \pm 0.0002\,{\rm km\,s^{-2}}$. The accuracy of our V_{rad} determinations is not as good as would be expected, and it is not easy to explain the degradation of the radial velocity correlation functions. Part of it undoubtedly results from the strong rotational broadening which spoils the steepest profile gradients, but there must be other sources of degradation; this could be small intrinsic variations of the photospheric spectra themselves. Most interestingly, the spectra show no distinctive signs of chromospheric activity except possibly in the very cores of strongly saturated lines. Another possible source of radial

velocity degradation is the dominance of terrestrial absorption lines in the red spectra. Whereas they help finding accurate radial velocities they are also relatively strong, and their appearance spoils even the well-developped line troughs as shown in Figs. 6 and 7.

3. Stellar parameters and spectrum synthesis

The basic data obtained from the binary orbit and the photometry in Table 1 can be employed to determine stellar parameters such as are commonly used to construct models of single star atmospheres. As noted above the mass and radius of the secondary subgiant lead to a *surface gravity* of $\log g = 3.67$. Our independent determination from spectrum synthesis results in $\log g = 3.65$, a value that will be used in the following analysis. The *effective temperature* cannot be determined in a straighforward manner. It is known since Kron (1947) that a substantial fraction of the stellar surface must be covered with dark spots similar to those found on the Sun. Current estimates of that fraction of the projected stellar surface are between 0.0 and 0.3 (e.g. Lanza et al. 1998). It is important to note that these spots with temperatures assumed between 3000 and 3500 K (Poe & Eaton 1985, Lanza et al. 1998) contribute in different ways to the *visual spectrum* and to the *luminosity* of the secondary. This is obvious when the *bolometric* luminosity is synthesized from the two surface components. Starting with the *visual* absolute magnitude of the secondary, $M_{V,2} = 3.6$, we assume that this magnitude combines the contributions of a surface fraction f_q covered by the quiet atmosphere and a fraction $f_s = 1 - f_q$ emerging from cool spots.

If we allowed only for a bolometric correction of the integral secondary spectral type, BC(K0 IV) ~ 0.15, the absolute bolometric magnitude would be $M_{bol,2} = 3.45$, and $4\,[T_{eff}] = [L] - 2\,[R]$ would lead to an effective temperature of $T_{eff} = 4800$ K, a value that has been used in previous investigations[2]. Such a low temperature is, however, clearly outside any reasonable interpretation of the observed line spectra. Instead, it is necessary to account for the fact that most of the flux produced by the *spots* is emitted in the far red and does not affect the visual magnitude. Estimating the spot temperature by $T_{eff,s} = 3000 \ldots 3500$ K and the effective temperature of the quiet atmosphere by $T_{eff,q} = 5000 \ldots 5200$ K, the flux ratios in the V band calculated from the respective Planck functions lead to a spot contribution between 5 and 1% of the total flux. Thus we correct the observed visual magnitude for an assumed surface fraction covered by spots and obtain a visual magnitude that would be observed if the *whole* stellar surface were covered by the quiet atmosphere[3]. The corresponding virtual brightness increase depends on the cool spot surface fraction f_s; for $f_s = 0.3$ the magnitude correction is $\Delta M_V = -0.38$, and $M_{V,2} = 3.22$. Applying a bolometric correction of BC = 0.25 ... 0.15 for K0 IV subgiants with temperatures $T_{eff,q}$ = 5000 ... 5200 K, $M_{bol} = 2.97 \ldots 3.07$. The effective temperatures for these *bolometric magnitudes* are between 5160 and 5040 K, roughly consistent with the temperatures assumed for the bolometric corrections. Assuming temperatures below 5000 K would require BC ~ 0.3; this results in $M_{bol} = 2.92$ and thus leads to a higher $T_{eff,q} = 5220$ K, in contradiction to the assumed temperature; this shows that the possible temperature variations circle around a mean temperature of 5100 K. A smaller surface fraction $f_s = 0.2$ leads to $M_V = 3.36$, and with a bolometric correction of 0.20 a consistent temperature is produced for $T_{eff,q} = 4930$ K; a larger fraction $f_s = 0.4$ implies $M_V = 3.05$, and with BC = 0.2 a considerably higher effective temperature, $T_{eff,q} \sim 5300$ K, is required. Both alternatives are only marginally compatible with the observed spectrum; in fact, only values around $f_s = 0.3$ fit perfectly to our observations.

Our approach to the abundance analysis of cool stars is based on spectrum synthesis. Synthetic spectra require the specification of atmospheric models which are represented here by line-blanketed flux-constant stratifications in hydrostatic, convective and local thermodynamic equilibrium. Such model atmospheres have been used for quite some time (Gehren 1977, Fuhrmann et al. 1997), and they produce nearly the same results as those of Kurucz (1992) taking into account his opacity distribution functions (ODF). All atmospheric models are specified in terms of the four parameters T_{eff}, $\log g$, [Fe/H], and v_t, where [Fe/H] refers to the *metal* abundance assuming for simplicity a solar (meteoritic) mixture. The determination of these parameters follows a well-defined scheme that makes use of the temperature sensitivity of the Balmer lines, the gravity sensitivity of the Mg I b lines, whereas [Fe/H] and v_t are fitted to the medium strong metal lines of ionized iron. There are a few ambiguities detected, and thus a number of spectral windows have been examined, the most important being the regions around Hα, the Hβ range, the Mg I b window, and the G band between 4250 and 4350 Å including the Hγ line. Further windows are added to obtain very rough estimates of other metal abundances. The surface gravity is in fact assumed known from both mass and radius of the secondary; therefore the value $\log g = 3.65$ has been adopted as the final parameter.

Spectrum synthesis is calibrated with the solar flux atlas of Kurucz et al. (1984) using the same line list as for the atmospheric models. In all spectral windows investigated, the numerous absorption lines were individually adjusted to fit the solar spectrum (considering up to a few thousand lines per window). Particular emphasis was attributed to the many weak lines including the contributions of a number of diatomic molecules. Yet there remain a few intervals in which even stronger lines have not been identified. A typical fit to the solar spectrum using LTE line formation with the same type of model atmosphere (i.e. *not* an empirical solar model) is shown in Fig. 1.

No other star is normally observed with such a high resolution, and it is therefore informative to examine the sensitivity with respect to changes of the individual stellar parameters of a solar-type spectrum that is broadened by a rotation velocity of $v_{rot} \sim 75\,\mathrm{km\,s^{-1}}$. This is displayed in Fig. 2, where the influence of temperature, gravity, and abundance variations

[2] The square brackets are defined by $[X] = \log(X_\star/X_\odot)$

[3] Note that this procedure is necessary only to relate the proper effective temperature to the unspotted atmosphere

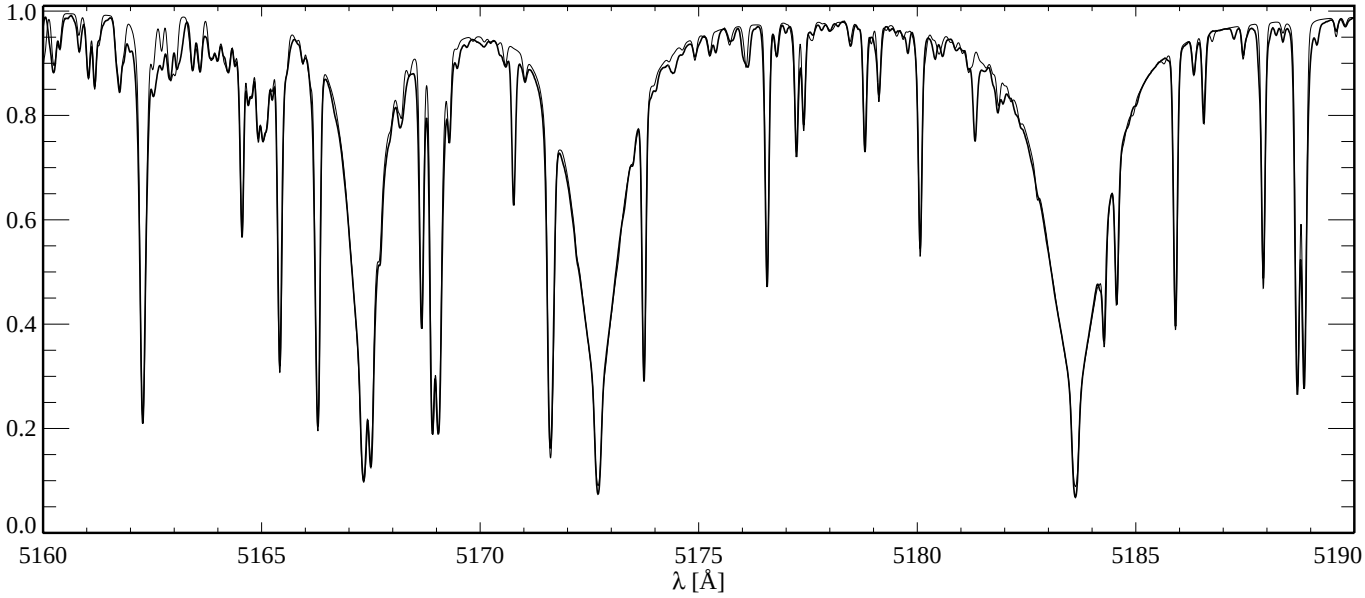

Fig. 1. The solar flux spectrum (Kurucz et al. 1984) near the Mg I b lines. The thin curve represents the fit to this spectrum using an ODF-blanketed model with solar parameters, $T_{eff} = 5780$ K, $\log g = 4.44$, [Fe/H] = 0.0, and $v_t = 1.2\,\mathrm{km\,s^{-1}}$, thoroughly adjusting f values and damping constants. Note the numerous molecular lines of C_2 and MgH; note also the missing lines near 5162, 5171 and 5181 Å

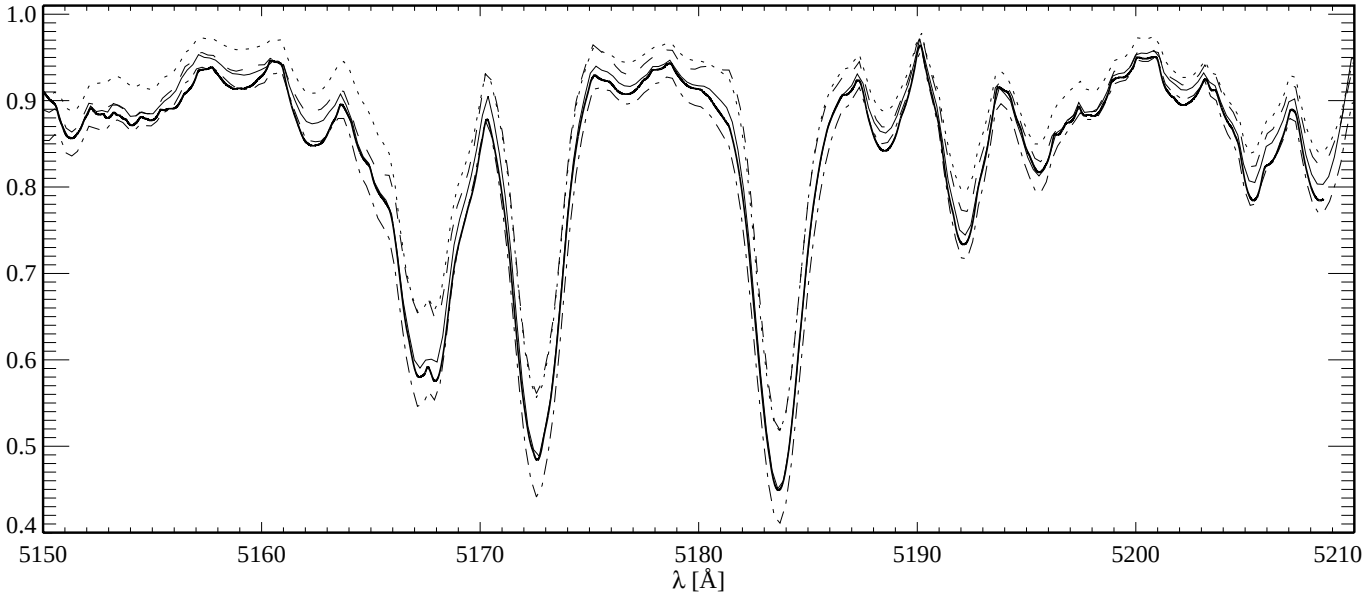

Fig. 2. The solar flux spectrum as displayed in Fig. 1, but convolved with a rotational profile corresponding to $v_{rot} = 75\,\mathrm{km\,s^{-1}}$. The synthetic spectra refer to the variation of $\Delta T_{eff} = -200$ K (dot-dashes), $\Delta \log g = -0.5$ (dashes), and Δ[Fe/H] = –0.3 (dots)

is demonstrated. It is evident from Fig. 2 that the influence of different parameter variations can be localized in the spectral window. This is even more pronounced in the spectrum synthesis of AR Lac below. We note that the solar spectrum when convolved with such a rotational profile loses its continuum positions which are normally detected with high resolution at a number of wavelengths. However, there remains a fundamental difference between *low-resolution* spectra that sample only one spectral element every 2 Å and a FOCES *high-resolution* spectrum that is sampled at a resolution of 0.2 Å but broadened to a 2 Å FWHM by rotation. Experience shows that the accuracy with which the solar spectrum must be fitted is inversely proportional to the resolution of the stellar spectrum to which the synthetic spectrum fits are applied.

With the improved line data obtained from solar spectrum synthesis it is now possible to extend the synthesis method to stars with different parameters, although it must be stated that the reference to the solar spectrum is not valid for all types of stars; in particular very cool stars of K and M spectral types with a significant part of their spectrum covered by molecular

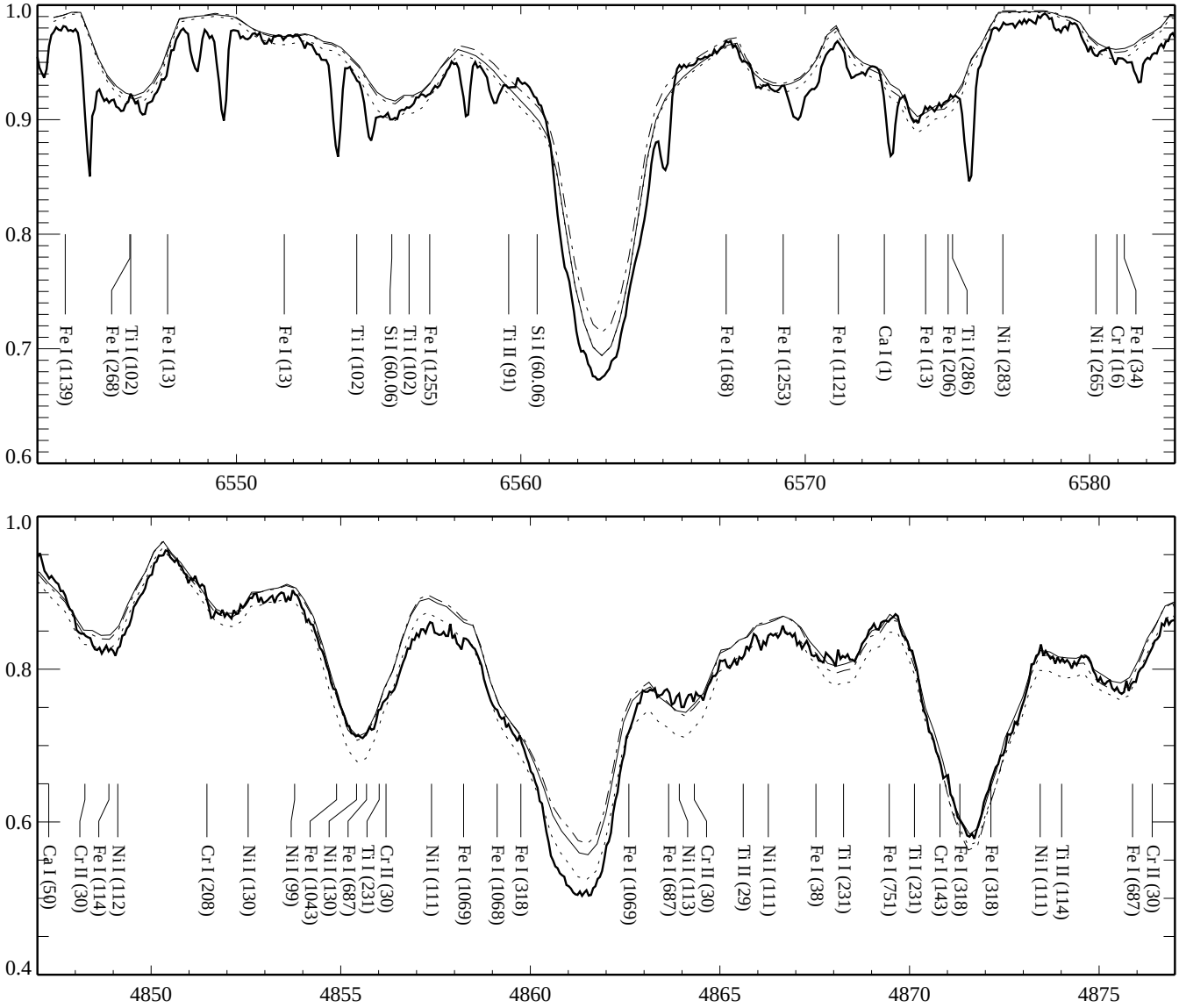

Fig. 3. *top:* AR Lac spectrum near Hα. The three single exposures are corrected for radial velocity variation and co-added (fat continuous curve). The sharp lines are due to terrestrial H_2O; their width reflects the radial velocity variation. The thin continuous spectrum shows the final fit with $T_{eff} = 5100$ K, $\log g = 3.65$, [Fe/H] = 0.0, and $v_t = 1.6\,\mathrm{km\,s^{-1}}$. The other synthetic spectra refer to the variation of $\Delta T_{eff} = -100$ K (dot-dashes), and Δ[Fe/H] = +0.2 (dots). All synthetic spectra are convolved with a rotational profile of $v_{rot} = 72\,\mathrm{km\,s^{-1}}$. *bottom:* AR Lac spectrum near Hβ. The synthetic spectra refer to the same parameters as above.

bands require an additional reference star. However, even a first glimpse on the spectrum of AR Lac shows that this subgiant is not very cool, and the spectral features are still similar to those seen in the Sun spectrum. As mentioned above, in the first step of the analysis it is necessary to determine the basic stellar parameters of AR Lac. The object observed here is the secondary component with *no* contribution of the primary (which is slightly fainter and completely occulted during all three exposures). Our estimates above also lead to the conclusion that the fraction of the stellar surface covered by cool spots is of the order of 30% corresponding to a spot *spectrum* contribution to the observed visual stellar continuum of roughly 2 ... 3%. Since no other evidence is available this flux fraction could be represented by e.g. the *sunspot* spectrum; the AR Lac spot contribution is so small, that its spectrum which is also strongly broadened by rotation can be represented as well by a constant fraction of the observed continuum flux. Note that such a cool spot flux fraction depends strongly on wavelength; thus it varies from 1% of the continuum at the G band to 1.5% at Hβ to 2% at Mg I b and 3% at Hα. For most of the spectral features this difference will not be observed since its amplitude is proportional to the line *depression* and thus visible only in the centers of saturated lines.

4. Photospheric abundances and discussion

Figs. 3 to 5 display the four standard spectral windows used to determine the basic parameters of AR Lac. We start their inter-

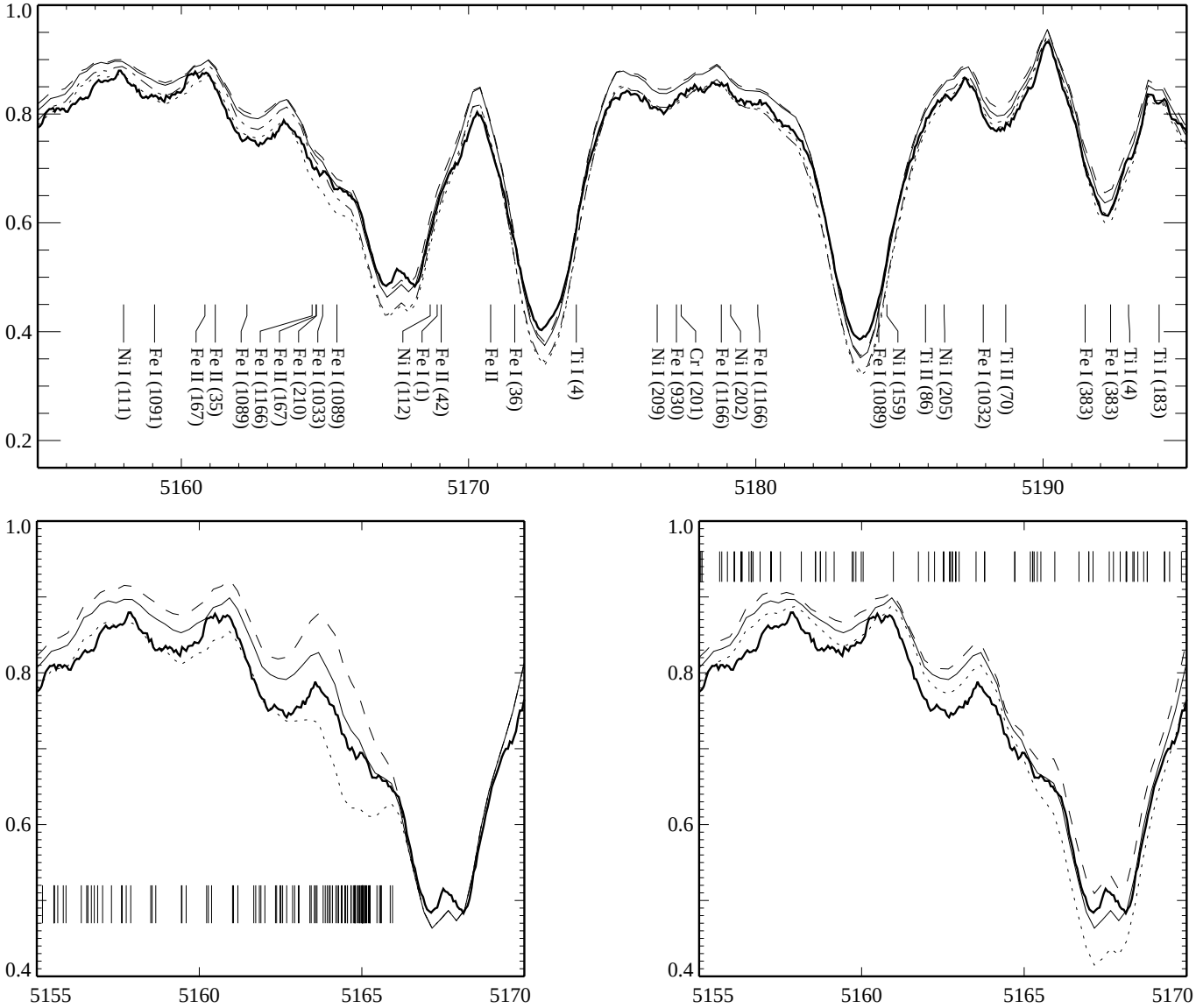

Fig. 4. *top:* AR Lac spectrum near the Mg I b lines (see the corresponding part of the solar spectrum in Fig. 1). The synthetic spectra refer to the same parameters as in Fig. 3, with an additional curve refering to the variation of the microturbulence parameter by $\Delta v_t = -0.4\,\mathrm{km\,s^{-1}}$ (long dashes). The thin continuous spectrum shows the standard fit with [C/Fe] = 0 and [Mg/Fe] = 0. *bottom:* Profile wings of Mg b line at 5167 Å. The left window demonstrates the influence of the C_2 band when varying the C abundance by ± 0.2 dex, the window on the right shows the variation of Mg Ib and the MgH lines with Mg abundance where Δ[Mg/H] = ± 0.2 dex. In both windows the positions of the respective molecular lines are indicated

pretation by noting that – for the purpose of spectrum synthesis – the continuum positions are unknown since the high rotational broadening efficiently hides continuum windows; the continuum position is therefore an additional free parameter. In spite of the low surface temperature the Hα window in Fig. 3 (top) is still sensitive to the *effective temperature* which would be fitted by $T_{eff} = 5100\,\mathrm{K}$ over most of the profile except the near wings at ± 3 Å. Since Hα is in principle the least blended line in the whole spectrum it should be fitted with the highest accuracy. There is no significant noise in this part of the spectrum, and every small-scale frequency variation must therefore be due to *terrestrial* features of which the stronger H_2O lines stand out clearly from the AR Lac continuum. All the faint modulations of the U-shaped rotation troughs are real and also due to H_2O. They are more readily visible in the single exposures in Fig. 7. Thus, any acceptable fit to this spectrum may not produce flux residuals *below* those observed. Postponing the discussion of the problem documented in the inner Hα wings we note that the other stellar parameters fit the observed spectrum with sufficient accuracy.

The Hβ window displayed in Fig. 3 (bottom) should provide an independent temperature estimate as much as Hγ does. This results from the different origins of the line broadening which for Hα is mostly due to *resonance broadening* by colli-

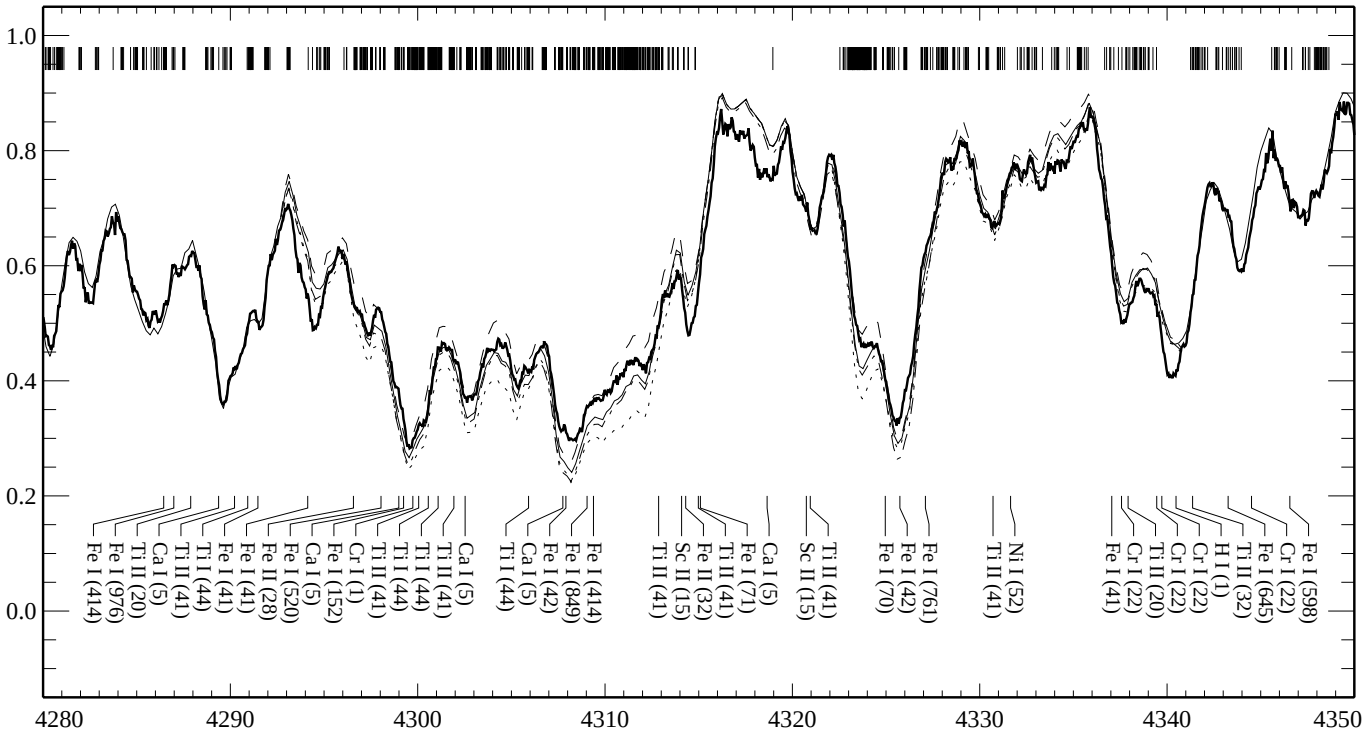

Fig. 5. AR Lac spectrum covering the G band. The thin continuous spectrum shows the final fit with [C/Fe] = 0. The other synthetic spectra refer to the variation of $\Delta T_{eff} = -100$ K (dot-dashes), and Δ[C/H] = +0.2 (dots) and –0.2 (long dashes), respectively. In addition to the stronger metal lines only the positions of the CH lines have been marked

sions with neutral hydrogen atoms whereas Hβ and the higher series members are broadened mainly by the *Stark effect*. The lines therefore have their origin in different layers of the stellar atmosphere (Fuhrmann et al. 1993): the wings of Hβ originate in optical depths $\overline{\tau} \sim 1$, and those of Hα also represent substantial contributions from $\overline{\tau} < 1$. The spectrum fit with the final parameters is at least as satisfactory as that of Hα when the line cores are ignored[4]. In fact, even the solar spectrum fit is unable to reproduce the very Balmer line cores because these emerge in part from *chromospheric* layers that are not represented by the photospheric models. The Hβ window also strongly emphasizes the dependence of the spectral fluxes on the metal abundance (where in this particular case [Fe/H] in fact refers to the *iron* abundance). A factor of 2 increase or decrease of the Fe abundance would not be compatible with most of the observed iron line spectrum in this window.

Fig. 3 makes it clear that at solar abundances and temperatures as low as 5100 K rotation can efficiently hide much of the Balmer lines' temperature sensitivity. Consequently, most of the necessary information is contained in the Mg I b window of Fig. 4. At these low effective temperatures the photospheric ionization equilibrium of magnesium becomes heavily weighted towards the Mg I state, and it reacts on any temperature change. At the same time the strong Mg line wings in the range of 5160 to 5167 Å become dependent on the atmospheric pressure and therefore on *surface gravity*. The C_2 lines in the bottom left panel make it relatively easy to distinguish between gravity and metal (carbon) abundance variations. In the synthesis calculations presented here we have for simplicity assumed that [Mg/Fe] = 0; this is confirmed by the wing-to-core ratios of the b lines in the bottom right panel. Part of that window between 5190 and 5205 Å is not reproduced here; it contains a large number of lines sensitive to the *microturbulence* velocity (similar to the region around Hβ). Together with some of the stronger lines these lines discriminate between microturbulence and metal abundance being responsible for profile broadening.

Fig. 5 shows a large part of the G band which can be successfully reproduced with [C/H] = [Fe/H] = 0; we note that the synthetic spectra are based on a spectrum fit to the solar flux spectrum that required the *individual* adjustment of all contribut-

Table 3. Final stellar parameters of AR Lac secondary component obtained during eclipse spectroscopy of the primary

v_{rot}	$73 \pm 3\,\mathrm{km\,s^{-1}}$	including macroturbulence	
$T_{\rm eff}$	5100 ± 100 K	surface without spots	
$\log g$	3.65 ± 0.05		
v_t	$1.6 \pm 0.3\,\mathrm{km\,s^{-1}}$		
[Fe/H]	0.0 ± 0.1	[Na/H]	0.15 ± 0.1
[Mg/H]	0.0 ± 0.1	[Ca/H]	0.1 ± 0.15
[Si/H]	0.1 ± 0.3	[Ba/H]	0.2 ± 0.2
[C/H]	0.0 ± 0.1		

[4] For strongly rotationally broadened stellar spectra the convolution of non-photospheric parts of the line profiles into the photospheric wings is an unsolved problem

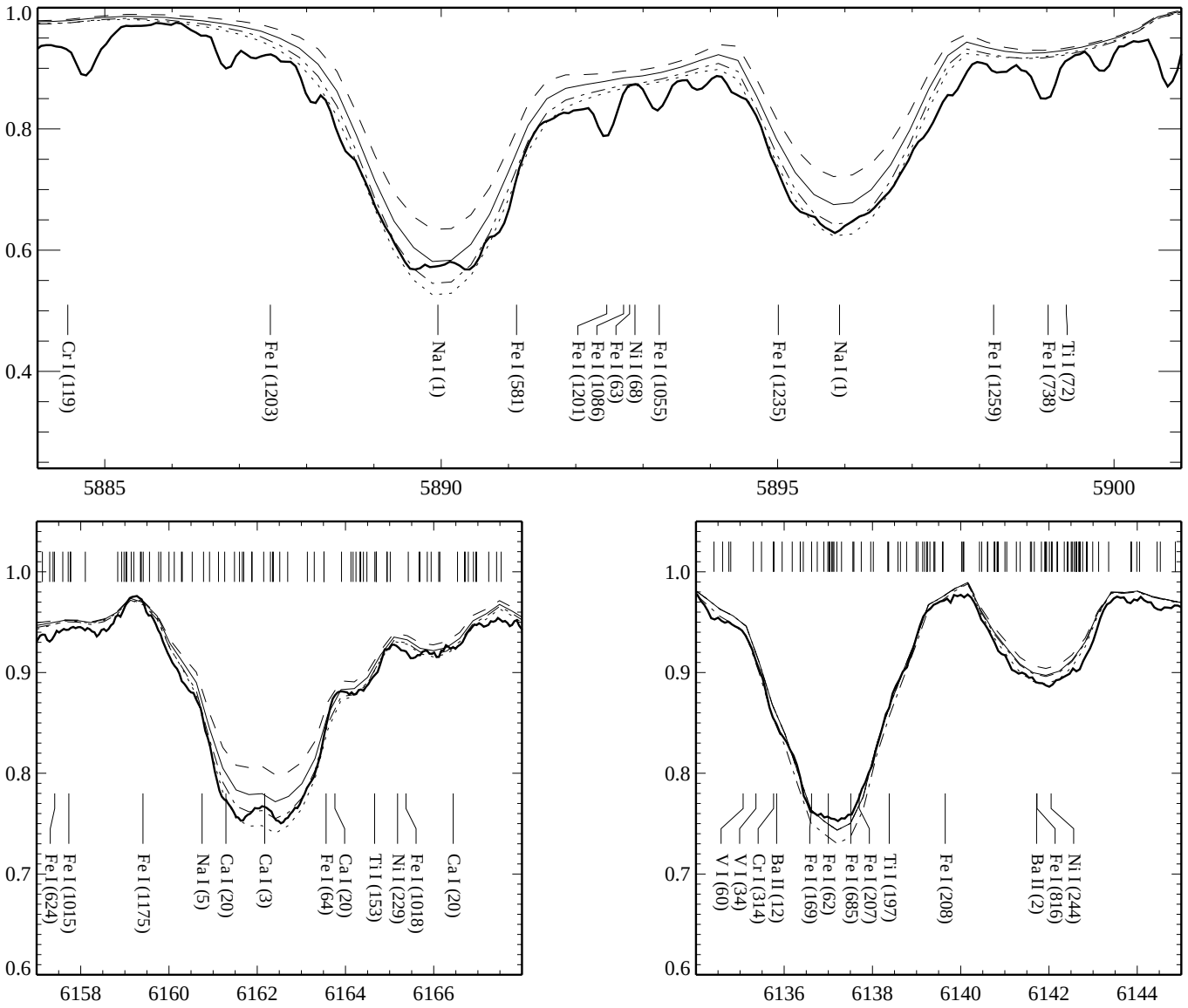

Fig. 6. *top:* AR Lac spectrum near Na I D lines. The thin continuous spectrum shows the fit with [Na/Fe] = 0. The other synthetic spectra refer to the variation of $\Delta T_{eff} = -100$ K (dot-dashes), and Δ[Na/H] = +0.2 (dots) and –0.2 (long dashes), respectively. *bottom:* Strong Ca I lines near 6160 Å(left), and Ba II line at 6142 Å(right). Synthetic spectra are the same as above, with dots and dashes refering to [Ca/H] and [Ba/H] abundance variations, respectively. Positions of C_2 lines are indicated

ing lines. Yet there are unexplained features between 4310 and 4320 Å that display the present shortcomings of both spectral line identifications and stellar atmosphere theory.

Silicon abundances have been estimated from a set of relatively strong lines near 7410 Å (spectrum not shown here). Na, Ca and Ba abundances are determined from the spectral windows shown in Fig. 6. All four elements seem to show slightly enhanced abundances as compared with the Sun. Deviation of the atmospheric excitation and ionization from LTE must play a marginal role in our analysis because AR Lac is not metal-poor. Recent calculations of Baumüller et al. (1998) indicate that in this region of the HR diagram the *true* (NLTE) abundance of Na tends to be between 0.02 and 0.05 dex *lower* than obtained from an LTE determination, and the work on Barium by Mashonkina et al. (1998) shows a similar tendency. Thus the proper abundances of Na and Ba may well be solar.

None of the spectral windows leads to a full set of fundamental stellar parameters by itself. It requires, however, little experience to disentangle the interdependence of the spectral regions on different parameters once the reliability of the spectrophotometry can be judged. This is where the superb quality of the FOCES échelle spectra is needed with their fully predictable order continua that represent a relative spectral flux accuracy better than 1%. Thus looking for the fits in different windows we conclude that the parameters given in Table 3 are the best overall data. We refrain from specifying more exact values for the abundances since this would require a considerable increase in spectral information input and methodical accuracy which, in

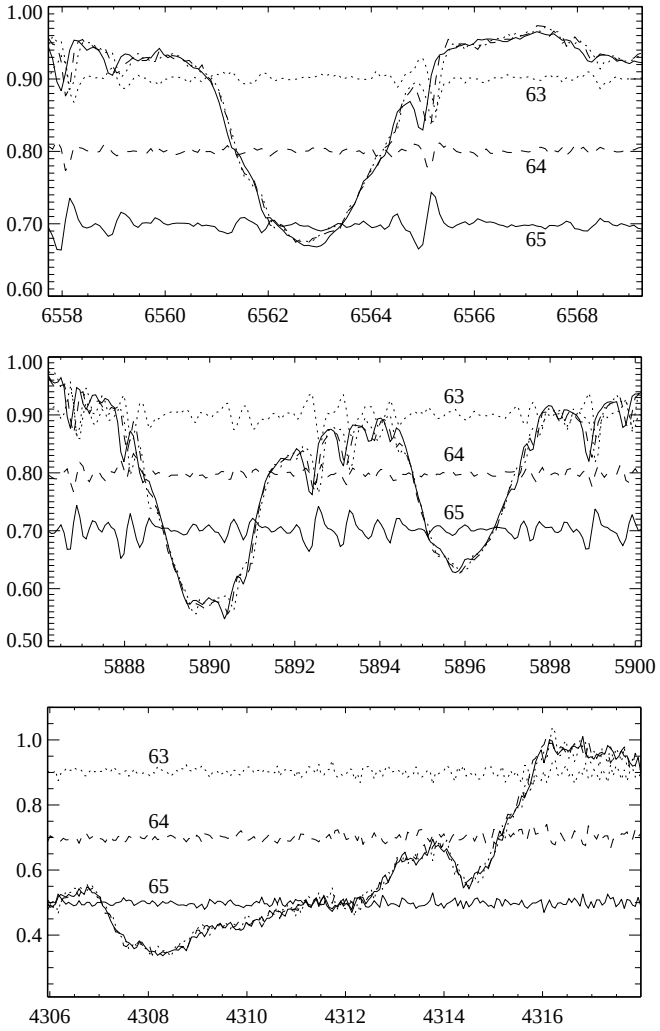

Fig. 7. The strongly varying spectra refer to the single exposures No. 63 (dots), 64 (dashes) and 65 (continuous) of Table 2 corrected for radial velocity variation. The small variations of the exposures with respect to a *mean spectrum* (not shown here) are represented as labeled curves, shifted by appropriate amounts to fit into the panels. Different panels include Hα (*top*), Na I D (*middle*), and part of the G band (*bottom*)

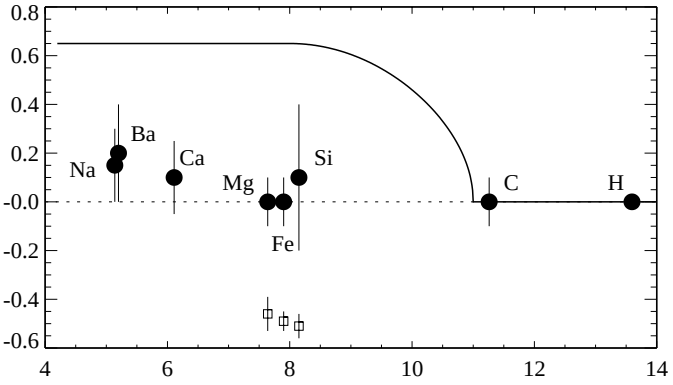

Fig. 8. Photospheric abundances as a function of the first ionization potential (filled circles, with error bars). The curve is a rough representation of the FIP effect as documented by Meyer (1993). Also shown are coronal abundances of Mg, Fe and Si from Kaastra et al. (1996, open squares)

turn, would require an even higher spectroscopic standard. As is now obvious the metal abundance represented by [Fe/H] is best determined in the Hβ window, and [Mg/H] comes mainly from the Mg I b lines. Variations of the carbon abundance are seen both in the C_2 lines in the Mg I window and in the CH lines of the G band. Note in particular the different run of carbon and metal abundance in the Mg I window.

4.1. Spectrum invariability

Although the interpretation of the spectrum synthesis results is straightforward, the discrepancy on the near wings of Hα remains. At first sight the selection of a lower temperature, e.g. $T_{\rm eff}$ = 4900 K, would seem to remove the problem with the line fit in the Hα window although the overall fit to the Balmer lines would become significantly worse. This could be adjusted by assuming a slightly lower spot surface fraction. However, turning to other windows such as Mg I b and the G band, it becomes evident that the resulting increase in core saturation of strong metal lines (the b lines themselves but also the strong lines near 4325 Å) cannot be compensated by a decrease of metal abundances.

Another reason for rejecting lower effective temperatures on the basis of the Hα wings alone is a possible spectrum variability reported by a number of observers. Bopp & Talcott (1978) have found the Hα core filled in during flare activity, Hα has been cited as showing variable emission by Goraya & Srivastava (1984). More evidence for variability of the Hα profile comes from Bopp & Talcott (1980) who find "presumably a randomly variable absorption profile", a result that was, however, not confirmed by Huenemoerder & Ramsey (1984). There has been no high-resolution confirmation of this kind of spectrum variability; the data of both Goraya & Srivastava and Huenemoerder & Ramsey are not conclusive, but if there were any spectrum variability in the residuals of Huenemoerder & Ramsey's Fig. 2c, it would be detected around $\pm 3 \ldots 4$ Å off the line center, i.e. exactly where our high-resolution Hα profile fit fails.

We have therefore analyzed our single exposures for spectrum variability; the results are documented in Fig. 7. Whereas the influence of terrestrial lines is evident in both Hα and Na I D exposures, all three windows definitely show *no evidence for variability of the stellar spectrum* during the eclipse observations. This does of course not rule out spectrum variability on a longer time scale but it leaves the strange profile shoulders of Hα unexplained.

4.2. Coronal and photospheric abundances

The photospheric abundances presented in Table 3 are not comparable in accuracy with the results usually obtained when analyzing normal stellar spectra of stars with low rotational velocities. The reason for this is obviously that abundances in the case of AR Lac are always obtained from synthesis of many

single lines blended together. The corresponding errors of the abundances make it difficult to give a detailed discussion of the star's chemical composition. Actually, all the photospheric abundances of AR Lac are in approximate agreement with a *solar* abundance mixture. There appears to be a slight enhancement in the abundances of Na, Ba, and Ca, but a fraction of that overabundance may well be due to our simple assumption of local thermodynamic equilibrium (see above).

Fig. 8 shows the discrepancy between the abundances derived from either photospheric or coronal line analyses. For the low FIP elements Mg, Fe and Si this discrepancy is clearly beyond the error bars. In particular, Fe and Mg definitely have solar photospheric abundances whereas the X-ray data are obviously subsolar. Most of the other coronal abundances are subsolar, too (Kaastra et al. 1996); thus on the basis of coronal abundances alone, a FIP effect must be ruled out. The same would hold for the photospheric abundances, if the FIP abundance curve of Meyer (1993) were used as reference. Unfortunately, the oxygen triplet near 7770 Å was outside the spectral coverage of our spectrograph; we are therefore unable to determine O abundances, and C is the only element with a reasonably high FIP in our analysis of the photospheric spectrum.

A direct comparison of photospheric and coronal abundance data shows agreement only for Ni which appears to be similar in both plasmas. However, this value is neither very strongly supported by our analysis nor by Kaastra et al. (1996). Therefore, our analysis does not resolve the current problem with the X-ray abundances.

References

Baumüller D., Butler K., Gehren T., 1998, A&A, in press
Bopp B.W., Talcott J.C., 1978, AJ 83, 1517
Bopp B.W., Talcott J.C., 1980, AJ 85, 55
Chambliss C.R., 1976, PASP 88, 762
Eaton J.A., Hall D.S., 1979, ApJ 227, 907
Fuhrmann K., Axer M., Gehren T., 1993, A&A 271, 451
Fuhrmann K., Pfeiffer M., Reetz J., Gehren T., 1997, A&A 323, 909
Gehren T., 1977, A&A 59, 303
Goraya P.S., Srivastava R.K., 1984, IBVS 2579
Gunn A.G., Hall J.C., Lockwood G.W., Doyle J.G., 1996, A&A 305, 146
Hall D.S., Kreiner J.M., 1980, Acta Astron. 30, 387
Hall D.S., Richardson T.R., Chambliss C.R., 1976, AJ 81, 1138
HIPPARCOS Catalogue, 1997, electronic version, CDS, Strasbourg
Huenemoerder D.P., Ramsey L.W., 1984, AJ 89, 549
Jetsu L., Pagano I., Moss D., et al., 1997, A&A 326, 698
Kaastra J.S., Mewe R., Liedahl D.A., et al., 1996, A&A 314, 547
Kron G.E., 1947, PASP 59, 261
Kurucz R.L., 1992, Rev. Mex. Astron. Astrofis. 23, 181
Kurucz R.L., Furenlid, I., Brault, J., Testerman, L., 1984, Solar Flux Atlas from 296 to 1300 nm. Kitt Peak National Solar Observatory
Lanza A.F., Catalano S., Cutispoto G., Pagano I., Rodonò M., 1998, A&A 332, 541
Mashonkina L., Gehren T., Bikmaev I., 1998, A&A, submitted
Meyer J.P., 1985, ApJS 57, 173
Meyer J.P., 1993, In: Prantzos N., Vangioni-Flam E., Cassé M. (eds.) Origin and Evolution of the Elements. Cambridge Univ. Press, Cambridge, p. 26
Ottmann R., Schmitt J.H.M.M., Kürster M., 1993, ApJ 413, 710
Ottmann R., Pfeiffer M.J., Gehren T., 1998, A&A, in press
Patterer R., Drake J., Vedder P., Craig N., Bowyer S., 1993, BAAS 25, 861
Pfeiffer M., Frank C., Baumüller D., Fuhrmann K., Gehren T., 1998, A&AS 130, 381
Poe C.H., Eaton J.A., 1985, ApJ 289, 644
Popper D.M., 1990, AJ 100, 247
Sanford R.F., 1951, ApJ 113, 299
Singh K.P., White N.E., Drake S.A., 1996, ApJ 456, 766
Solanki S.K., 1996, In: Strassmeier K.G., Linsky J.L. (eds.) Stellar Surface Structure. Kluwer Publ., Dordrecht, p. 201
Strassmeier K.G., Hall D.S., Fekel F.C., Scheck M., 1993, A&AS 100, 173
Walter F.M., Gibson D.M., Basri G.S., 1983, ApJ 267, 665
White N.E., Shafer R.A., Horne K., Parmar A.N., Culhane J.L., 1990, ApJ 350, 776
White N.E., Arnaud K., Day C.S.R., et al., 1994, PASJ 46, L97